Targeting *Pf*CLK3 with Covalent Inhibitors: A Novel Strategy for Malaria Treatment

Skye B. Brettell,[1] Omar Jahna,[2] Abbey Begen,[3] Gillian Cann,[3] Niniola Olaniyan,[2] Saumya Sharma,[3] Tamas Yelland,[4] Alison J Hole,[4] Benazir Alam,[4] Ross Gillespie,[1] Michael Capper,[1] Graeme Milligan,[2] David J Clarke,[5] Andrew B. Tobin,[2]✉ Andrew G. Jamieson[1] ✉

[1]School of Chemistry, The Advanced Research Centre, University of Glasgow, 11 Chapel Lane, G11 6EW, U.K. [2]Centre for Translational Pharmacology, The Advanced Research Centre, University of Glasgow, 11 Chapel Lane, G11 6EW, U.K. [3]KelticPharma Therapeutics, The Advanced Research Centre, University of Glasgow, 11 Chapel Lane, G11 6EW, U.K. [4]Evotec(UK) Ltd, 95 Park Drive, Milton Park, Abingdon, Oxfordshire, OX14 4RY, U.K. [5]EaSTCHEM School of Chemistry, University of Edinburgh, Joseph Black Building, David, Brewster Road, Edinburgh, EH9 3FJ, U.K. ✉e-mail: andrew.tobin@glasgow.ac.uk; andrew.jamieson.2@glasgow.ac.uk

Abstract

Malaria continues to pose a significant global health threat, with the number of deaths exceeding 600,000 annually. Acquired resistance to frontline drugs by the most deadly parasite, *Plasmodium falciparum*, means this number is increasing each year. There is therefore an urgent unmet need for new medicines with novel mechanisms of action. In this work, we solved the co-crystal structure of the essential malarial kinase *Pf*CLK3 with the reversible inhibitor TCMDC-135051 **1**. This facilitated the rational design of covalent inhibitors of this validated drug target. An allosteric cysteine residue (Cys368) that is poorly conserved in the human kinome was targeted to improve the selectivity of hit molecules. Structure-based drug design yielded chloroacetamide **4**, which displays low nanomolar potency and covalent inhibition in both

recombinant protein and *P. falciparum* killing assays. Efficacy in parasites was maintained when **4** was washed out 6 hours after exposure. Compound **4** showed significantly improved kinase selectivity relative to TCMDC-135051 **1**, and cell viability experiments in HepG2 cultures also demonstrated an over 500-fold selectivity index relative to *P. falciparum* parasites. To our knowledge, compound **4** represents the first covalent inhibitor of a malarial kinase. Its covalency, efficacy and selectivity for *Pf*CLK3 makes it a promising lead in the search for a single-dose cure for malaria.

Introduction

Despite effective artemisinin-based combination therapies (ACTs), >240 million cases of malaria infection are reported annually resulting in >600,000 deaths.[1] These numbers, although high, are a significant improvement on 2015 levels and represent some degree of success in the World Health Organisation "Global Technical Strategy (GST)" aimed at reducing the global burden of malaria in 2030 by 90% from 2015 levels. Whereas the reduction in malaria cases can be attributed to the early success of the GTS, the last 5 years has seen little change in infection rates and in some areas of the world the trend has even been reversed and infections have increased. This worrying trend has been attributed to the acquired resistance of the *Anopheles* mosquito vector to the insecticides used to impregnate bed nets and the emergence of parasite resistance to current frontline antimalarials, including ACTs.[2,3] It is now widely understood that if the world is to avoid significant increases in cases of malaria, particularly of the most virulent human malaria species *Plasmodium falciparum* (*P. falciparum*), new chemotherapeutic agents that act through a novel mechanism of action are urgently required.

To address this, we have focused on targeting malaria parasite protein kinases that we identified as essential for blood stage parasite survival.[4] Emerging from these studies has been a focus on the *P. falciparum* cyclin-dependent like protein kinase-3 (*Pf*CLK3), one of a family of 4 protein kinases with a role in the phosphorylation and assembly of components of the spliceosome.[5] A screen of the GlaxoSmithKline anti-malarial focused chemical library, called the Tres Cantos Anti-Malarial Set (TCAMS), identified the compound TCMDC-135051 **1 (Fig. 1)** as a selective *Pf*CLK3 inhibitor. This tool inhibitor was used in combination with genetically engineered parasite lines and field isolates to validate *Pf*CLK3 as a target with the potential to deliver a cure for blood stage infection, as well as preventing the development of gametocytes responsible for transmission and parasiticidal activity of liver stage in a manner that can be prophylactic. TCMDC-135051 (**1**) has since entered a drug development programme aimed at generating a clinical candidate that is curative, transmission blocking and offering prophylaxis across *Plasmodium sp*.[6]

One of the major challenges faced in developing next generation anti-malarials is the requirement to produce a single dose medicine that is highly tolerated and safe to be administered to young children and pregnant women. That the erythrocytic stage of the parasite has a 48 hour cycle **(Fig. 1)**; that the parasite can sequester in tissue such as bone marrow; that the gametocyte stages can take many days to develop; and that stage V gametocytes remain in the circulation for several weeks, means that any effective anti-malarials need to act at multiple stages of the parasite life cycle for long periods.[7-9] Whereas inhibitors of *Pf*CLK3 are effective at multiple parasite stages, correlating with the importance of RNA-splicing in the biology of the parasite, the question of long exposure at the target is an important issue.[5] A potential strategy to deliver extended exposure is to build in favourable pharmaco-dynamic properties through the

application of covalent inhibitors, which irreversibly bind to the target.[10] This approach has been employed in targeting protein kinases in oncology, where covalent inhibitors have shown increased potency, selectivity and decreased propensity to resistance. Despite the unquestionable success of targeting protein kinases in cancer, the exploitation of protein kinase inhibitors in malaria is in its infancy.[11] What has certainly never been explored is the potential of covalent kinase inhibitors as effective anti-malarials.[12,13]

Here we employ a high-resolution atomic structure of TCMDC-135051 (**1**) in complex with *Pf*CLK3 to inform structure-guided design of a covalent inhibitor that targets a non-conserved cysteine residue proximal to the catalytic site of *Pf*CLK3. Protein mass spectrometry and live parasite wash-out experiments confirmed successful covalent modification of the target cysteine. The covalent *Pf*CLK3 inhibitor showed extended parasiticidal potency in the nanomolar range, as well as significantly improved selectivity over the human kinome and a more favourable cell viability profile in HepG2 cells when compared to the parent molecule TCMDC-135051 **1**. We conclude that a covalent binding mechanism for protein kinase inhibitors targeting essential malarial protein kinases could provide the pharmacodynamic and parasiticidal properties desired in a strategy for the development of a single dose cure for malaria.[12,14]

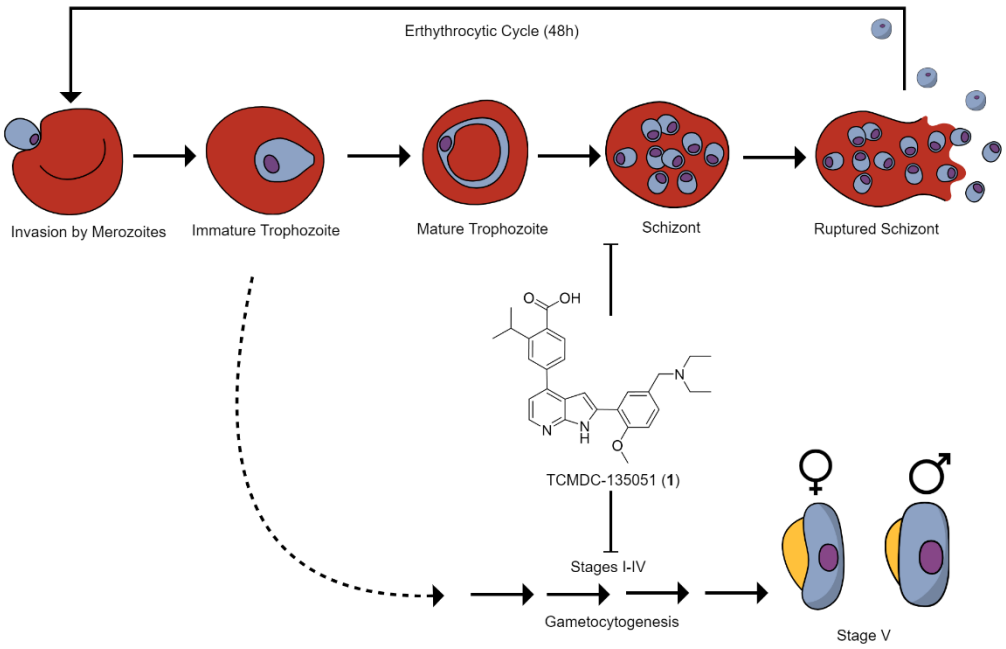

Figure 1: Inhibition of the *P. falciparum* life cycle at multiple stages by TCMDC-135051. Previous work [5] has established TCMDC-135051 (**1**) as a curative, transmission blocking and prophylactic agent, active in both asexual and sexual blood stages of the *P. falciparum* life cycle.

Results

X-ray crystal structure reveals the mechanism of TCMDC-135051 (1) / *Pf*CLK3 binding and facilitates structure-based covalent inhibitor design

To establish the binding mode of the tool *Pf*CLK3 inhibitor TCMDC-135051 (**1**) we report here a co-crystal structure of *Pf*CLK3 kinase domain in complex with TCMDC-135051 (**1**) to 2.1 Å resolution (**Fig. 2a, b,** PDB: 8RPC). The structure resembles our previously published [5] molecular modelling of TCMDC-135051 (**1**) in a homology model (generated using SWISS-MODEL and the kinase domain structure of the closest mammalian orthologue PRPF4B as a template) with an RMSD of 1.08 Å, yet with several important differences (**Fig. 2c, d**). The azaindole scaffold of TCMDC-135051 (**1**) binds as predicted to the ATP-binding site, in the

flipped orientation, forming hydrogen bonds with the amide backbone of Met447 (**Fig. 2c, d**).[15] However, the core sits closer to the hinge loop and further out of the binding site than predicted, which allows the diethylamine to form a charge-dipole interaction in the crystal structure with the backbone carbonyl of Trp448 (**Fig. 2c-e**). The carboxylic acid-Lys394 interaction predicted in the docking studies is mediated by three water molecules as seen in the crystal structure (**Fig. 2c**), which sit in the pocket forming a network of interactions with three other residues Cys510, Asp511 and Ser377 (**Fig.2f**). Interestingly, the isopropyl group does not displace these waters to sit in the hydrophobic pocket next to the Phe444 gatekeeper as predicted (Fig. **2d**). Surprisingly, this lipophilic functionality appears to protrude out of the pocket towards the solvent exposed space (**Fig. 2c**).

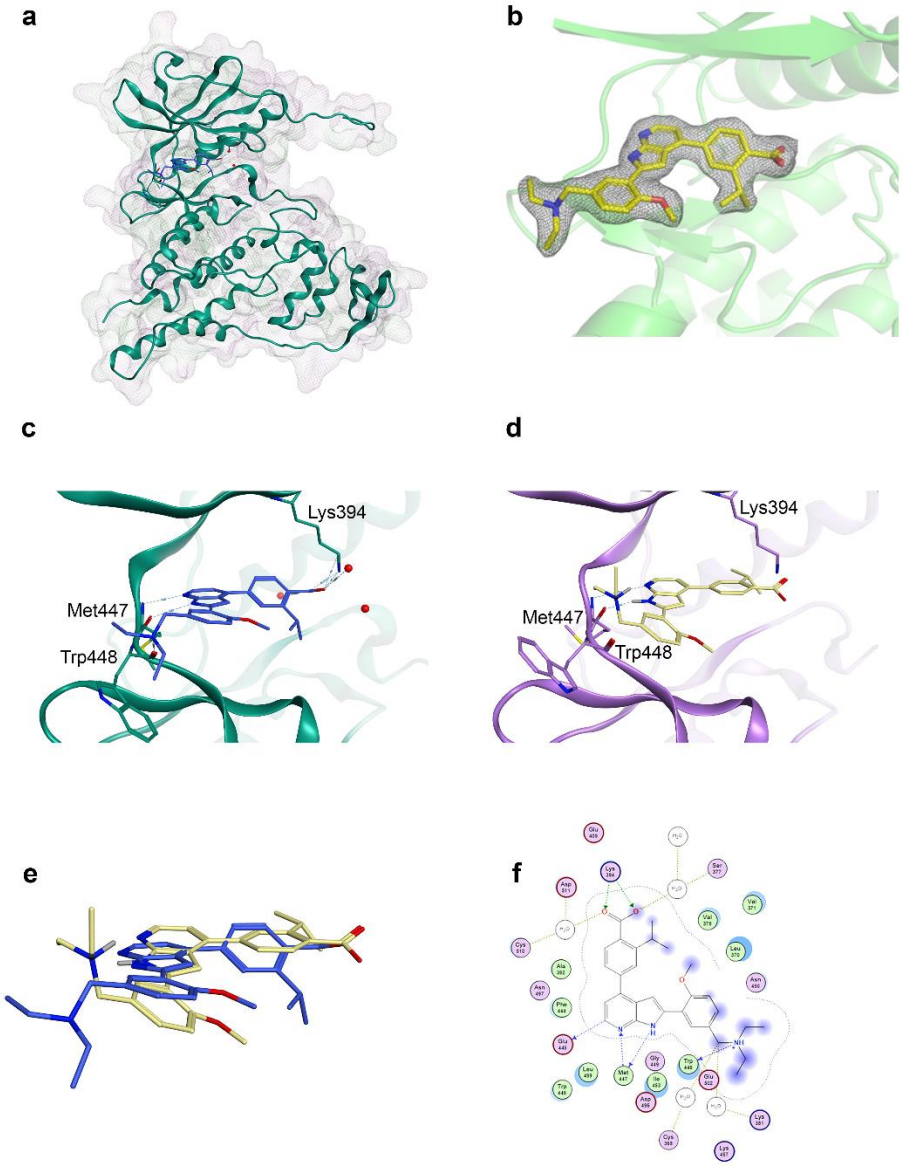

123 **Figure 2: Mechanism of *Pf*CLK3 inhibition by TCMDC-135051 a,** Co-crystal structure of
124 *Pf*CLK3 (teal) in complex with TCMDC135051 (blue) (PDB: 8RPC). Protein surface mesh
125 visualized in MOE, hydrophobic patches in green and hydrophillic in lilac. **b,** Electron density
126 map for TCMDC-135051 (yellow) in the ATP binding site (green). **c,** ATP binding site
127 interactions of TCMDC-135051 (blue) evident in co-crystal structure with *Pf*CLK3 (teal). **d,**
128 Molecular docking of TCMDC-135051 (yellow) in a previously published homology model of

*Pf*CLK3 (lilac).[6] **e**, Overlay of TCMDC-135051 binding pose from 8RPC (blue) and molecular docking (yellow). **f**, Ligand interaction map of TCMDC-135051 in co-crystal structure 8RPC.

Using this structure, two cysteines were identified within or near the ATP binding site (**Fig. 3a**): Cys368 of the P loop and Cys510, the DFG-1 residue of the activation loop.[16] Sequence and structural alignments of *Pf*CLK3 and a set of 497 human kinases were completed using the resource KINCORE™ and the Molecular Operating Environment (MOE) (**Fig. 3b**).[17,18] All cysteines within the P-loop of the human kinome set were selected in KINCORE and the structures of these kinases loaded and aligned with *Pf*CLK3 in MOE. This analysis established that Cys510 (DFG-1) of *Pf*CLK3 has 45 equivalent cysteines within the human kinome set, whereas Cys368 has only 2 (hCDK8 and hCDK19, **Fig. 3b**). Cys368 was therefore chosen as the more attractive nucleophilic residue for a covalent inhibitor to confer selectivity.

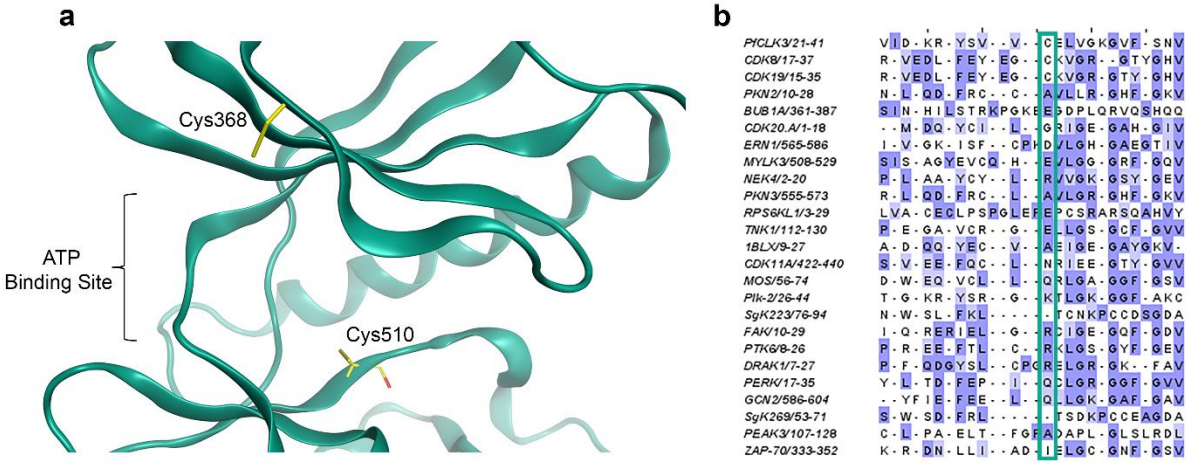

Figure 3: Potential *Pf*CLK3 cysteine residue targets. a, Cysteine residues (yellow) located near the ATP binding site of *Pf*CLK3 (teal). Cys510 is the DFG-1 residue located on the activation loop, while Cys368 is located adjacent to the P-loop. **b**, Sequence alignment of all P-loop cysteines in the human kinome against *Pf*CLK3 (row 1, teal box). Only 2 kinases, CDK8 and CDK19 (rows 2 and 3, teal box) possess cysteines in locations equivalent to Cys368 of

*Pf*CLK3. Cys368 resides in an allosteric site, outside the ATP-pocket, towards the N terminus of the P-loop. From the crystal structure, the diethylamine moiety of TCMDC-135051 (**1**), which projects towards the solvent exposed space, is oriented near Cys368. Analogs were therefore designed from the TCMDC-135051 (**1**) scaffold via a piperazine linker, a natural extension of the diethylamine, to orientate warheads towards the target residue (**Fig. 4a**). The isopropyl group from TCMDC-135051 (**1**) was omitted to reduce the molecular weight and lipophilicity, given this group was previously found to be non-essential for kinase inhibition.[6]

A series of analogs was designed featuring warheads of increasing reactivity (**Fig. 4a**). Compound **2** features an acrylamide, the most common of the electrophiles due to its low reactivity.[19,20] Compound **3** features a basic amino-acrylamide warhead, while compound **4** incorporates an α-chloroacetamide.[21,22] These warheads show increasing reactivity when matched molecular pairs are reacted with glutathione, with the α-chloroacetamide being the most reactive.[19] All analogs were then docked into the co-crystal structure (8RPC). **2**-**4** were predicted to maintain the binding mode of TCMDC-135051 (**1**), forming the same key interactions discussed above, while projecting sufficiently out of the pocket to form covalent bonds with Cys368 (**Fig. 4b**).

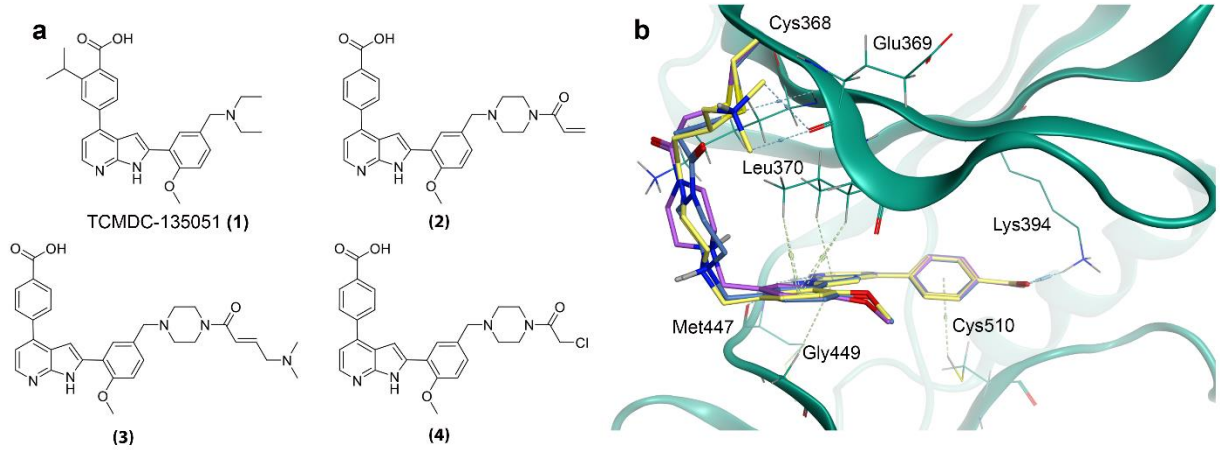

161

162 **Figure 4: Compound design and molecular docking. a,** Clockwise from top left- TCMDC-
163 135051 (**1**), unsubstituted acrylamide **2**, basic dimethylamino acrylamide **3**, and chloroacetamide
164 **4**. **b**, molecular docking of compounds **2** (blue), **3** (yellow) and **4** (purple) in the co-crystal
165 structure of TCMDC-135051 and *Pf*CLK3.

166 **Chemical synthesis of covalent inhibitors of *Pf*CLK3**

167 The three covalent analogs of varying reactivity were synthesised from a common intermediate,
168 the Boc-amine protected methyl ester **10** (**Scheme S1**). Compound **10** was obtained from a five-
169 step synthesis based on that of the hit compound TCMDC-135051 (**1**).[6] After global deprotection
170 of **10**, warheads were coupled onto the piperazine linker using standard amide coupling
171 conditions (**Scheme S2**). This yielded three molecules with presumed varying reactivity, as well
172 as a non-covalent control analogue **12** with the non-electrophilic acetyl cap on the piperazine
173 linker.

174 **Mass Spectrometry reveals specific covalent modification of the target cysteine**

Covalent adduct formation was investigated by intact protein mass spectrometry. Apo protein kinase domain was compared with samples which had been incubated with compounds **2**, **3** and **4** at varying pHs. These experiments were performed on *Pf*CLK3 kinase domain (334-699) given the full-length recombinant protein did not ionize using ESI TOF analysis. At physiological pH 7.4, no covalent adduct formation was observed for compound **2** after 4 hours. When the pH was raised to pH 9, adduct formation was observed. This implies a lack of warhead reactivity, with basic conditions required to deprotonate Cys368, increasing nucleophilicity and driving product formation. Cysteine reactivity is governed by the side chain pKa, which can vary from 3.5 to 12 depending on specific protein microenvironments.[23,24] Cys368 can therefore be considered to be relatively weakly nucleophilic. The more reactive also substituted acrylamide **3** demonstrated no adduct formation at pH 7.4, while the most reactive chloroacetamide **4** demonstrated 100% singular adduct formation (**Fig. 5a**).

The nucleophilic target residue was then determined by tandem mass spectrometry (**Fig. 5b-e).** After incubation with compound **4**, *Pf*CLK3 was digested with trypsin. The resulting peptides were then analysed by electrospray ionisation mass spectrometry and compared with the list of expected peptides using Protein Prospector.[25] This yielded four peptides modified by the expected monoisotopic mass of compound **4** minus Cl (**Fig. 5b**), with one principal peptide being >10-fold greater in abundance, YSVVCELVGK. This peptide corresponds to residues 364-373 (**Fig. 5e**). This ion was then further fragmented by CID to reveal a single modification on Cys368 (**Fig. 5c,d**). Given that the chloroacetamide **4** appears to form only one covalent adduct in the intact mass spectrometry (**Fig 5a**), and that the modified peptide YSVVCELVGK is detected in much greater ion abundance than other modified species (**Fig 5b**), this implies

selectivity for Cys368. This is presumably aided by the pseudo-high concentration in the ATP binding site due to the reversible interactions of the ligand.

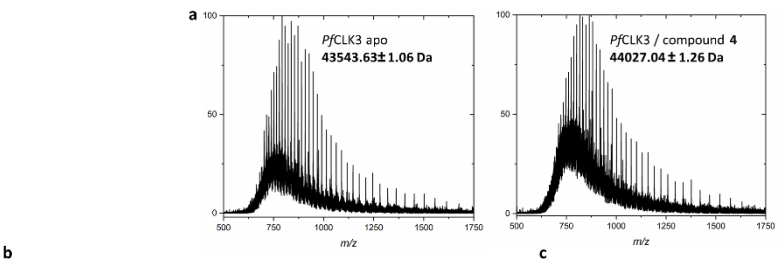

b

Unmodified Tryptic Peptides Matched

Theoretical Mass	Observed Mass	Delta ppm	Start	End	Missed Cleavages	Ion Abundance	Sequence
592.3453	592.3465	2.05	172	176	0	2827631	(K)FNALK(V)
626.4236	626.425	2.23	57	62	0	3177505	(K)IPVAVK(V)
660.4291	660.4303	1.9	98	103	0	3096738	(R)LLSSIK(Y)
666.3643	666.3658	2.15	318	322	0	13365344	(K)MQFLK(K)
674.4236	674.425	2.11	232	237	0	16309838	(K)ILFPGK(S)
702.4396	702.4412	2.32	77	82	0	15539142	(K)EISILK(K)
814.3838	814.3853	1.9	245	250	0	17812274	(K)LMMEYK(G)
847.4308	847.4318	1.16	357	363	0	2055476	(R)ESIHFSK(S)
860.5352	860.5372	2.26	143	149	0	31192208	(K)QLFIALR(H)
863.4985	863.5011	3.02	42	49	0	131095480	(K)GVFSNVLK(C)
915.5146	915.5177	3.44	327	334	0	20490972	(K)QLGDLLEK(C)
1015.5935	1015.5954	1.9	202	210	0	357419040	(R)APEIILGFR(Y)
1028.6099	1028.6118	1.85	290	298	0	10176803	(R)VISDLRPTK(N)
1044.587	1044.589	1.93	335	343	1	12157347	(K)CLILDPSKR(Y)
1096.5707	1096.5727	1.84	32	41	0	9691016	(R)YSVVCELVGK(G)
1117.6034	1117.6052	1.62	22	31	1	43221568	(K)AMVGEVIDKR(Y)
1156.6936	1156.6959	1.99	325	334	1	8491315	(K)IKQLGDLLEK(C)
1415.6074	1415.6123	3.51	364	375	0	10532679	(K)SQNEGSENLYFQ(-)
1479.7698	1479.7735	2.47	50	62	1	11258921	(K)CYDMVNKIPVAVK(V)
1601.8071	1601.8104	2.08	344	356	0	128200720	(R)YTPDQALQHPYLR(E)
1775.8785	1775.8836	2.86	299	312	0	878649856	(K)NITCDLLEHQYWLK(G)
1805.8388	1805.8434	2.56	128	142	0	29971568	(K)YGNGHGLNATAVHCYTK(Q)
1863.9997	1864.0033	1.92	156	171	0	454097216	(R)IMHADLKPDNILINEK(F)
1917.9251	1917.9309	3.02	106	120	0	48147072	(K)NHLCLVFEWMWGNLR(I)
2209.0834	2209.0891	2.59	104	120	1	12392040	(K)YKNHLCLVFEWMWGNLR(I)
2256.1183	2256.1265	3.65	211	231	0	349820224	(R)YDAQIDVWSAAATVFELATGK(I)
2358.1129	2358.1224	3.99	177	198	0	49509384	(K)VCDLGSASDISENEITSYLVSR(F)
2449.1207	2449.1277	2.85	260	279	0	478936192	(K)GGQFYSQHFNENLDFLYVDR(D)

Modified Tryptic Peptides Matched

m/z Submitted	MH+ Matched	Delta ppm	Start	End	Missed Cleavages	Ion Abundance	Sequence
1370.6843	1370.6813	3.4	335	342	0	4692249	(K)CLILDPSK(R)
1578.7699	1578.7661	3.42	32	41	0	622064192	(R)YSVVCELVGK(G)
2258.0799	2258.0739	3.34	299	312	0	18998020	(K)NITCDLLEHQYWLK(G)
2288.0393	2288.0342	2.83	126	142	0	4378855	(K)YGNGHGLNATAVHCYTK(Q)

c

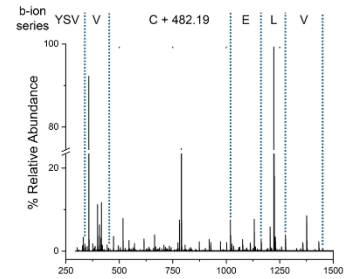

d

	Fragment Ion	Theoretical Mass	Observed Mass	Error (ppm)	
YSV	B3	349.1638	349.1636	-0.51	
V	B4	448.2322	448.2319	-0.55	
C(*)	B5	1033.4368	1033.4363	-0.48	
E	B6	1162.4794	1162.4788	-0.50	
L	B7	1275.5634	1275.5629	-0.45	
V	B8	1374.6318	1374.6313	-0.36	
G	B9	1431.6533	1431.6529	-0.29	
K					
	Y3	302.1954	302.1952	-0.60	VGK
	Y4	415.2795	415.2792	-0.61	L
	Y5	544.3220	544.3218	-0.46	E
	Y6	1129.5266	1129.5260	-0.56	C(*)
	Y7	1228.5951	1228.5945	-0.45	V
	Y8	1327.6635	1327.6630	-0.36	V
	Y9	1414.6955	1414.6953	-0.16	S
					Y

e

```
  1  MTTGNNANLS DNWNDSEGYY KAMVGEVIDK RYSVVCELVG KGVFSNVLKC YDMVNKIPVA
 61  VKVIRDNDMM KKAAEKEISI LKKLNQYDKD NKRHIIRLLS SIKYKNHLCL VFEWMWGNLR
121  IALKKYGNGH GLNATAVHCY TKQLFIALRH MRKCRIMHAD LKPDNILINE KFNALKVCDL
181  GSASDISENE ITSYLVSRFY RAPEIILGFR YDAQIDVWSA AATVFELATG KILFPGKSNN
241  HMIKLMMEYK GKFSHKMIKG GQFYSQHFNE NLDFLYVDRD HYSKKEVVRV ISDLRPTKNI
301  TCDLLEHQYW LKGNSPKMQF LKKKIKQLGD LLEKCLILDP SKRYTPDQAL QHPYLRESIH
361  FSKSQNEGSE NLYFQ
```

Figure 5: Protein mass spectrometry of *Pf*CLK3 and compound 4. **a**, Intact protein mass spectrometry of apo *Pf*CLK3 and *Pf*CLK3 incubated with compound **4** for 4 hours. A mass difference of 483.41 can be observed, corresponding to the mass of compound **4** less the chloride leaving group. **b,** Table of unmodified and modified peptides obtained from the tryptic digest. **c,** CID fragmentation spectrum of the most abundant modified peptide, YSVVCELVGK which contains Cys368. **d,** Table of fragmentation ions masses quoted as the monoisotopic

neutral mass. **e,** The sequence of *Pf*CLK3 kinase domain with the modified peptide in bold and Cys368 highlighted in yellow.

***In vitro* potency against recombinant *Pf*CLK3 demonstrates improved activity for covalent binding mode**

Compounds **1**, **4** and **12** were then evaluated for inhibitory activity against recombinant full-length *Pf*CLK3 in an *in vitro* TR-FRET protein kinase assay. To test the effect of covalency, three different concentrations of the natural substrate ATP were used: 5 μM (K_m), 500 μM and 3 mM (to mimic cellular levels).[26] The hypothesis being that once a covalent inhibitor has bound to the target protein, it cannot be outcompeted by ATP. Biochemical potencies demonstrated exactly this: while compound **4** and its non-covalent control exhibited comparable potencies to TCMDC-135051 when [ATP] = K_m, (pIC_{50} = 8.02 and 7.93, p = 0.88 and 0.37 respectively), TCMDC-135051 and non-covalent compound **12** both decreased in potency when ATP concentrations rose. TCMDC-135051 demonstrated decreased potencies of 7.06 ($p <$ 0.0001 *wrt* K_m) and 6.35 ($p <$ 0.0001 *wrt* K_m) for 500 μM and 3 mM ATP respectively, with compound **12** showing a similar trend (pIC_{50} = 6.05 and 5.32, $p <$ 0.0001 *wrt* K_m). Chloroacetamide **4** however maintained its high potency in all assays, where pIC_{50} = 7.69 (p = 0.1158 *wrt* K_m) and 7.66 (p = 0.0658 *wrt* K_m) for [ATP] = 500 μM and 3 mM respectively. While ATP non-competitive data may often suggest an allosteric binding mode, the comparison with ATP-competitive compound **12,** combined with mass spectrometry data, is indicative of a covalent binding mode for compound **4**. It is supposed this binding mode may be advantageous relative to TCMDC-135051 in cellular assays, when ATP concentrations rise to 1-3 mM.[26]

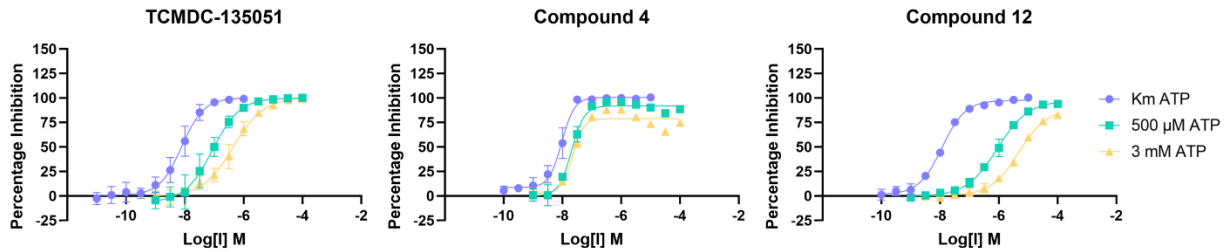

ATP Concentration	TCMDC-135051	Compound 4	Compound 12
Km (5 µM)	8.11 ± 0.18	8.02 ± 0.14	7.93 ± 0.04
500 µM	7.06 ± 0.23	7.69 ± 0.06	6.05 ± 0.11
3 mM	6.35 ± 0.15	7.66 ± 0.03	5.32 ± 0.10

Figure 6: In vitro activity of compounds 4, 12 and TCMDC-135051 (1) against recombinant *Pf*CLK3 shows maintained potency for covalent compound 4 when ATP concentrations reflect cellular levels. Each compound was tested for inhibitory activity with ATP concentrations = Km (5 µM, purple), 500 µM (teal) and 3 mM (yellow). While TCMDC-135051 (**1**) (left) and compound **12** (right) lost potency with increased ATP concentrations, compound **4** retained its activity. pIC_{50} values and standard deviations are given in the table.

Chloroacetamide **4** was also evaluated using a thermal shift assay. In the presence of an excess of **4**, full-length *Pf*CLK3 was highly thermodynamically stable, with a 20 °C shift in Tm compared to the DMSO control (**Table S2**). This large shift demonstrates an impressive stabilisation effect of chloroacetamide **4**'s binding to *Pf*CLK3.

Evaluation of parasiticidal activity of compounds 1 and 4 confirms covalent-based mechanism of action

Covalent chloroacetamide inhibitor **4** and its non-covalent control analog **12** were next evaluated for parasiticidal activity in *P. falciparum* 3D7 cell line (**Fig. 7, Fig. S4**). After incubation with ring-stage parasites for 72 hours, chloroacetamide **4** exhibited a half-maximal response concentration (pEC_{50}) of 7.10. Compound **4** therefore has comparable potency to TCMDC

135051 (**1**) (pEC_{50} = 6.89, p = 0.5669) and a significant increase in potency compared to the non-covalent control compound **12** (pEC_{50} = 4.87, p < 0.0001, **Fig. S4**).

It was predicted that a covalent inhibitor may need only a short exposure to have a prolonged parasiticidal effect, whilst a non-covalent inhibitor would be less active after a short exposure. To test this notion parasites at ring stage were exposed for 6 hours only with compound **4** (covalent), and TCMDC-135051 (**1**) (non-covalent). Following compound washout the parasite culture was continued for 66 hours and parasite viability tested. Under these conditions the potency of TCMDC-135051 (**1**) significantly reduced (pIC_{50} = 5.91, p = 0.0003, **Fig. 7a**) whilst the potency of compound **4** was not reduced following wash out (**(**pIC_{50} = 7.04, p = 0.9439, **Fig. 7b)**. These data are consistent with a covalent mechanism of action in parasite cells for chloroacetamide inhibitor **4**. Furthermore, the demonstration of a short exposure time resulting in a prolonged parasiticidal effect is a useful finding in the quest for a single-dose cure for malaria.

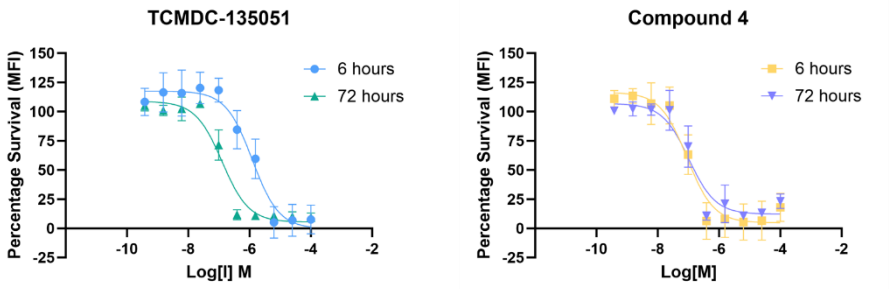

Incubation Time	TCMDC-135051	Compound 4	Compound 12
72 hours	6.89 ± 0.10	7.10 ± 0.21	4.87 ± 0.01
6-hour washout	5.91 ± 0.20	7.04 ± 0.15	NT

Figure 7: Parasiticidal activity of TCMDC-135051 and compound 4 reflects covalent binding mechanism and extended duration of action in cells. Compounds **1** and **4** were incubated with ring stage parasites for 72 hours (teal and lilac, respectively). In wash-out studies

(blue and yellow, respectively), compound medium was exchanged for compound-free medium after 6 hours, and parasites were incubated for a further 66 hours. While TCMDC-135051 (left) showed reduced potency after washout compared to the 72 hour incubation, compound **4** (right) maintained its potency. pEC_{50} values and standard deviations are given in the table.

Covalent targeting of Cys368 leads to increase in kinome selectivity

Compounds **2**-**4** were designed to improve the selectivity of TCMDC-135051 (**1**) by targeting a poorly conserved cysteine, Cys368. Chloroacetamide **4** was therefore screened against a representative panel of 58 human kinases from across the kinome, using Eurofins Discovery's *KinaseProfiler* technology. **Fig. 8a** compares the selectivity scores ($S_{(50)}$, $S_{(30)}$ and $S_{(20)}$) of **4** and TCMDC-135051 (**1**). $S_{(x)}$ represents the fraction of kinases with less than x% remaining activity when treated with 1 μM compound. These data show compound **4** to have a significant improvement in selectivity relative to TCMDC-135051 (**1**), with no kinases being inhibited below 20% remaining activity at 1 μM, and only 1 kinase below 30% activity (**Fig. 8a, Table S3**). Kinases inhibited below 50% activity by compound **4** are shown on the human kinome phylogenetic tree (**Fig. 8b**).[27] This implies that targeting of Cys368 can improve selectivity for *Pf*CLK3 over the human kinome. Furthermore, using the KINOME*scan*™ technology (**Fig. S6**), chloroacetamide **4** showed no substantial binding against CDK8 and CDK19, the two human kinases with equivalent cysteines (K_d > 30 μM). These data suggest that both reversible and irreversible interactions are driving selectivity of **4**, given that kinases with equivalent nucleophiles but different ligand pockets are unable to bind this molecule.

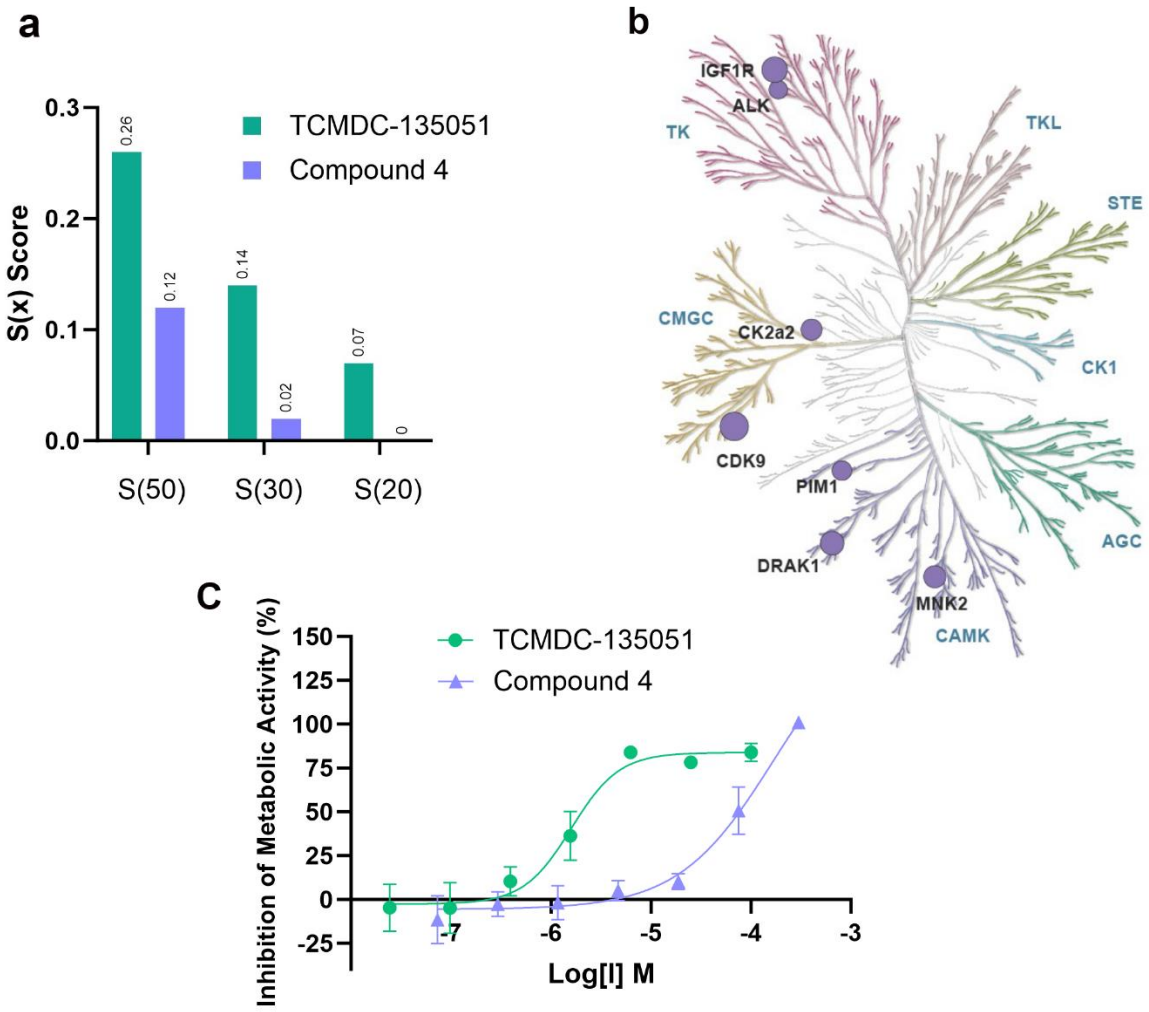

Figure 8: Compound 4 shows excellent selectivity profile compared to TCMDC-135051 (1). **a,** Selectivity scores of compound **4** and TCMDC-135051 (**1**) when screened against the 58 human kinases of the Eurofins KinaseProfiler™ Diversity panel. S(x) = number of kinases inhibited below x% activity when incubated with 1 µM compound/ number of kinases in the panel. Compound **4** is more selective than TCMDC-135051 (**1**), with a 5-fold improved S(30) score and zero kinases inhibited below 20% original activity. **b**, Human kinases inhibited ≥ 50% activity when exposed to 1 µM compound **4** highlighted in the human kinase phylogenetic tree. The size of the purple circle is proportional to the % inhibition. **c**, Inhibition of metabolic activity

of HepG2 cells. When incubated for 48 hours with HepG2 cells, compound **4** (pEC_{50} <4.20) proved substantially less cytotoxic than TCMDC-13501 (**1**) (pEC_{50} 5.80 ± 0.14),

Chloroacetamide covalent inhibitor 4 demonstrates exquisite selectivity index for parasites over human cells

Cell viability experiments for compound **4** and TCMDC-135051 (**1**) were conducted using human hepatocyte-like HepG2 cells, and both demonstrated low toxicity. HepG2 cells originate from the liver, which is particularly relevant for malaria given this is where the exo-erythrocytic cycle takes place.[28] Targeting the stage in the parasite life cycle that invades the liver is important to deliver a prophylactic treatment for malaria. Chloroacetamide **4** only fully inhibited metabolic activity of HepG2 cells at the highest concentration assessed (300 μM) (log[I] = -3.5, **Fig. 8**), with solubility issues restricting exposure to higher concentrations. While an accurate pEC_{50} could not therefore be calculated, this data demonstrates chloroacetamide **4** to be much less cytostatic than TCMDC-135051 (**1**) with pEC_{50} = 5.8. This is hypothesised to be explained in part by the increase in kinase selectivity afforded by targeting Cys368. Compound **4** therefore demonstrates an excellent selectivity index for 3D7 parasites over human cells, potentially representing a very large therapeutic window.

Discussion

The global effort to combat malaria has seen significant progress, yet challenges persist, particularly with emerging resistance to current frontline antimalarials and insecticides.[1] As a result, novel chemotherapeutic agents are urgently needed to address the stagnation in infection reduction and even the resurgence observed in some regions.[2,3] We targeted the malaria parasite protein kinase *Pf*CLK3, essential for blood stage parasite survival, as a potential avenue for

329 therapeutic intervention.[5] Our approach involved the identification and validation of *Pf*CLK3 as
330 a promising target for malaria treatment, culminating in the discovery of TCMDC-135051 (**1**) as
331 a selective inhibitor.[5,6] In this study, we leveraged this tool compound, and embarked on a drug
332 development program aimed at generating a pre-clinical candidate with curative, transmission-
333 blocking, and prophylactic properties across *Plasmodium* species.

334 One of the key challenges in developing next-generation antimalarials lies in ensuring
335 efficacy across multiple stages of the parasite's life cycle while maintaining safety, particularly
336 for vulnerable populations such as young children and pregnant women.[29,30] Given the complex
337 dynamics of parasite biology, including its 48-hour erythrocytic cycle and sequestration in
338 tissues, the development of a single-dose medicine with prolonged activity presents a formidable
339 task. Our study addressed this challenge by exploring the potential of covalent kinase inhibitors,
340 a strategy previously unexplored in the context of malaria. Given the success of covalent kinase
341 inhibitors in oncology, we believe this strategy could be harnessed in the malaria field. Though
342 one-third of approved targeted covalent inhibitors target infectious diseases, this does not include
343 the greatest parasitic killer.[12] The increased duration of action attributed to an irreversible
344 mechanism and increased selectivity can allow for smaller and less frequent dosing, which may
345 improve patient compliance- a significant issue in the treatment of malaria.[31,32] The ability of
346 covalent inhibitors to evade mutation events which lead to resistance also make them ideal
347 candidates for malaria eradication.[12,31]

348 Through high-resolution structural elucidation and molecular modeling, we identified a
349 non-conserved cysteine residue (Cys368) proximal to the ATP pocket of *Pf*CLK3 as a suitable
350 target for covalent inhibition. Subsequent synthesis and evaluation of covalent analogues
351 revealed improved parasiticidal potency, selectivity over the human kinome, and enhanced cell

viability profiles compared to the parent molecule, TCMDC-135051 (**1**). Importantly, our findings suggest that covalent binding mechanisms offer pharmacodynamic and parasiticidal properties conducive to the development of a single-dose cure for malaria.

The specificity of our covalent inhibitor of *Pf*CLK3 over human kinases, demonstrated through kinase profiling and binding assays, underscores the potential for selective targeting of the parasite while potentially minimising off-target effects. Moreover, the exquisite selectivity index of the lead compound, chloroacetamide **4**, for parasites over human cells highlights its promise as a therapeutic candidate with a large therapeutic window.

Notably, our study also provides insights into the mechanism of action underlying the prolonged parasiticidal effect of this covalent inhibitor. By comparing the activity of chloroacetamide **4** and non-covalent TCMDC-135051 (**1**) following short exposure and washout, we observed sustained potency with the covalent inhibitor, suggesting a mechanism whereby a brief exposure leads to prolonged parasite suppression.

Finally, we believe that our findings shed light on the potential of covalent kinase inhibitors as a novel strategy for malaria treatment. To the best of our knowledge, chloroacetamide **4** represents the first covalent kinase inhibitor of malaria, as well as a rare example of a covalent inhibitor of a non-human kinase.[13] By targeting essential malarial protein kinases such as *Pf*CLK3, covalent inhibitors offer a promising avenue for the development of safe and effective antimalarials with curative, transmission-blocking, and prophylactic properties. Further preclinical and clinical studies are warranted to validate the efficacy and safety of these compounds, with the ultimate goal of advancing towards global eradication of malaria.

Online content

Any methods, additional references, Nature Research reporting summaries, source data, extended data, supplementary information, acknowledgements, peer review information; details of author contributions and competing interests; and statements of data and code availability are available online.

References

1. World Malaria Report 2023. Geneva: World Health Organisation; 2023. Licence: CC BY-NC-SA 3.0 IGO.
2. Ashley, E.A. *et al*. Spread of Artemisinin Resistance in Plasmodium falciparum Malaria. *NEJM,* **371**, 411-423 (2014).
3. Menard, D. & Dondorp, A. Antimalarial Drug Resistance: A Threat to Malaria Elimination. *Cold Spring Harb. Perspect. Med,* **7**(2017).
4. Solyakov, L. *et al*. Global kinomic and phospho-proteomic analyses of the human malaria parasite Plasmodium falciparum. *Nat. Commun.* **2**, 1-12 (2011).
5. Alam, M.M. *et al*. Validation of the protein kinase *Pf*CLK3 as a multistage cross-species malarial drug target. *Science* **365**, 884-+ (2019).
6. Mahindra, A. *et al*. Development of Potent PfCLK3 Inhibitors Based on TCMDC-135051 as a New Class of Antimalarials. *J. Med. Chem.* **63**, 9300-9315 (2020).
7. Bozdech, Z. *et al*. The transcriptome of the intraerythrocytic developmental cycle of *Plasmodium falciparum PLoS Biol.* **1**, 85-100 (2003).

8. Oelschlegel, A.M. *et al*. Beyond the microcirculation: sequestration of infected red blood cells and reduced flow in large draining veins in experimental cerebral malaria. *Nat. Commun.* **15** (2024).
9. Josling, G.A. & Llinas, M. Sexual development in *Plasmodium* parasites: knowing when it's time to commit. *Nat. Rev. Microbiol.* **13**, 573-587 (2015).
10. Kim, H., Hwang, Y.S., Kim, M. & Park, S.B. Recent advances in the development of covalent inhibitors. *RSC Med. Chem.* **12**, 1037-1045 (2021).
11. Cabrera, D.G. *et al*. Plasmodial Kinase Inhibitors: License to Cure? *J. Med. Chem.* **61**, 8061-8077 (2018).
12. Kulkarni, S., Urbahns, K. & Spangenberg, T. Targeted Covalent Inhibitors for the Treatment of Malaria? *ACS Infect. Dis.* **6**, 2815-2817 (2020).
13. Alves, E.T.M., Pernichelle, F.G., Nascimento, L.A., Ferreira, G.M. & Ferreira, E.I. Covalent Inhibitors for Neglected Diseases: An Exploration of Novel Therapeutic Options. *Pharmaceuticals,* **16** (2023).
14. White, N.J., Nosten, F.H. SERCAP: is the perfect the enemy of the good? *Malar J* 281 (2021).
15. Irie, T. & Sawa, M. 7-Azaindole: A Versatile Scaffold for Developing Kinase Inhibitors. *Chem. Pharm. Bull.* **66**, 29-36 (2018).
16. Chaikuad, A., Koch, P., Laufer, S.A. & Knapp, S. The Cysteinome of Protein Kinases as a Target in Drug Development. *Angew. Chem., Int. Ed. Engl.* **57**, 4372-4385 (2018).
17. Modi, V. & Dunbrack, R.L., Jr. A Structurally-Validated Multiple Sequence Alignment of 497 Human Protein Kinase Domains. *Sci. Rep.* **9** (2019).

18. ULC, C.C.G.: M*olecular Operating Environment (MOE)*. 2020.0901 edn (910-1010 Sherbrooke St. W., Montreal, QC H3A 2R7, Canada, 2020).

19. Lonsdale, R. *et al.* Expanding the Armory: Predicting and Tuning Covalent Warhead Reactivity. *JCIM.* **57**, 3124-3137 (2017).

20. Roskoski, R., Jr. Properties of FDA-approved small molecule protein kinase inhibitors: A 2022 update. *Pharm. res.* **175**, 106037-106037 (2022).

21. Flanagan, M.E. *et al.* Chemical and Computational Methods for the Characterization of Covalent Reactive Groups for the Prospective Design of Irreversible Inhibitors. *J. Med. Chem.* **2014** 57 (23), 10072-10079

22. Tsou, H.R. *et al*. 6-Substituted-4-(3-bromophenylamino)quinazolines as putative irreversible inhibitors of the epidermal growth factor receptor (EGFR) and human epidermal growth factor receptor (HER-2) tyrosine kinases with enhanced antitumor activity. *J. Med. Chem* **44**, 2719-2734 (2001).

23. Liu, R., Yue, Z., Tsai, C.-C. & Shen, J. Assessing Lysine and Cysteine Reactivities for Designing Targeted Covalent Kinase Inhibitors. *JACS.* **141**, 6553-6560 (2019).

24. Bak, D.W., Bechtel, T.J., Falco, J.A. & Weerapana, E. Cysteine reactivity across the subcellular universe. *Curr. Opin. Chem. Biol*. **48**, 96-105 (2019).

25. Protein Prospector (RRID:SCR_014558). (University of California at San Francisco).

26. Teng, R. *et al*. Metabolite profiling of the intraerythrocytic malaria parasite *Plasmodium falciparum* by ^{1}H NMR spectroscopy. *NMR Biomed.* **22**, 292-302 (2009).

27. Eid, S., Turk, S., Volkamer, A., Rippmann, F. & Fulle, S. KinMap: a web-based tool for interactive navigation through human kinome data. *BMC Bioinform.* **18** (2017).

28. Maier, A.G., Matuschewski, K., Zhang, M. & Rug, M. *Plasmodium falciparum*. *Trends in Parasitol.* **35**, 481-482 (2019).

29. Siqueira-Neto, J.L. *et al*. Antimalarial drug discovery: progress and approaches. *Nat. Rev. Drug Discov*. **22**, 807-826 (2023).

30. Reader, J. *et al.* Multistage and transmission-blocking targeted antimalarials discovered from the open-source MMV Pandemic Response Box. *Nat. Commun.* **12**(2021).

31. Abdeldayem, A., Raouf, Y.S., Constantinescu, S.N., Moriggl, R. & Gunning, P.T. Advances in covalent kinase inhibitors. *Chem. Soc. Rev*. **49**, 2617-2687 (2020).

32. Bruxvoort K, Goodman C, Kachur SP, Schellenberg D. How patients take malaria treatment: a systematic review of the literature on adherence to antimalarial drugs. *PLoS One.* 2014 Jan 20; 9(1): e84555.

33. Vonrhein, C. *et al.* Data processing and analysis with the *autoPROC* toolbox. *Acta Crystallogr. D.* **67**, 293-302 (2011).

34. Tickle & I.J., F.C., Keller P., Paciorek W., Sharff A., Vonrhein C., Bricogne G. STARANISO. (Global Phasing Ltd., Cambridge, United Kingdon, 2018-2022).

35. McCoy, A.J. *et al. Phaser* crystallographic software. *J. Appl. Crystallogr.* **40**, 658-674 (2007).

36. Agirre, J. *et al.* The *CCP4* suite: integrative software for macromolecular crystallography. *Acta Crystallogr. D.* **79**, 449-461 (2023).

37. Jumper, J. *et al*. Highly accurate protein structure prediction with AlphaFold. *Nature* **596**, 583-+ (2021).

38. Smart, O.S., S.A., Holstein J., Womack T.o., Flensburg, C., Keller, P., Paciorek, & W., V., C., Briogne, G., Grade2 version 1.5.0. version 1.5.0. edn (Global Phasing Ltd.,

Cambridge, United Kingdom, 2021).

39. Emsley, P., Lohkamp, B., Scott, W.G. & Cowtan, K. Features and development of *Coot*. *Acta Crystallogr. D.* **66**, 486-501 (2010).

40. Bricogne, G., B.E., Brandl M., Flensburg C., Keller P., Paciorek W., Raversi P., & Sharff A., S.O.S., Vorhein C., Womack T.O. BUSTER version 2.11.8. edn ((1) Global Phasing Ltd., Cambridge, United Kingdom, 2017).

Methods

Protein Purification. A previously described full-length *Pf*CLK3 construct was expressed in *E. coli* strain C43 (DE3).[5] Protein was purified using IMAC, TEV cleavage, a second IMAC step before dialysing the protein into a final buffer containing 20 mM HEPES pH 7.4, 150 mM NaCl, 1 mM TCEP and 1 mM $MgCl_2$.

*Pf*CLK3 kinase domain (residues 334-699 with a C-terminal TEV cleavage sequence and His6-tag) was cloned into pFastBac vector and expressed and purified from Sf21 insect cells. Cells were infected using P2 BIICs at an MOI of 0.2 and left to express for 72 hours. Harvested cells were lysed and centrifuged before purifying using IMAC and SEC in a final buffer containing 20 mM HEPES pH 7.4, 150 mM NaCl, 1 mM TCEP and 1 mM MgCl2.

Crystallisation and structure determination. Freshly purified *Pf*CLK3 kinase domain was concentrated to 6.8 mg/mL, incubated with 0.5 mM TCMDC-135051 for 1 hour before centrifuging and setting up crystal trays. Crystals grew at 4 °C in a condition containing 2 M ammonium sulphate, 0.2 M potassium sodium tartrate tetrahydrate and 0.1 M sodium citrate pH 5.6. Crystals were cryo-protected in the reservoir solution supplemented with 10% v/v ethylene glycol and 10% v/v glycerol before flash freezing in liquid nitrogen.

Data was collected at the IMCA-CAT beamline at the APS and processed using autoPROC[33] and STARANISO[34]. Molecular replacement was performed using PHASER[35] of the CCP4 program suite[36] using the AlphaFold[37] model of *Pf*CLK3 kinase domain as a search model. Ligand restraints were generated using Grade2[38]. Iterative rounds of model building and refinement was performed using Coot[39] and BUSTER[40].

Computational Molecular Docking. All molecular docking was performed using MOE 2020.0901, using their in-house Amber10:EHT forcefield. Crystal structure 8RPC prepared using the "Quickprep" function in MOE. The ATP binding site was defined by "Compute" > "Sitefinder" > "Apply". "Dummy atoms" were then created to characterize the binding site.

All ligands were drawn in ChemDraw and their 3D structure was minimised using MOE. Protomers were generated by "Compute" > "Prepare" > "Protomers". Prepared ligands were saved to the working directory.

For covalent docking, one "dummy atom" created using the Site Finder tool was moved to sit adjacent to Cys368, and dummies were used to define the binding site. The reactive site was set to "selected atoms" and the thiol of Cys368 was selected in the visualiser. The beta-mercapto carbonyl 1,4-addition reaction was selected, and "Rigid Receptor" refinement was used. The "Complex" field from the results database was then copied into MOE for each ligand. The ligands "Tag" was changed to that of the receptor in the System Manager, and the complex was minimised using the "Quick Prep" function, with "Structure Preparation" and "Protonate3D" options deselected. This minimised covalent complexes which could then be analysed using the S score, E_conf, binding pose and observed clash.

Small-molecule synthesis and characterisation. Small molecules mentioned in this study were synthesised, with their purity and identity validated using ^{1}H & ^{13}C NMR, HPLC and HRMS. Methods and characterisation of newly synthesised small molecules are supplied in the Chemical Synthesis and Characterisation Data section of the Supplementary Information.

Trypsin digest and MS analysis of modified peptides. After incubation with a 5-fold excess of compound **4** for one hour as described above, 1.2 µL DTT (final concentration 1 mM) was added

to quench excess inhibitor. 2 µL of Pierce™ trypsin protease (1 mg/mL) was added to give a final protein: trypsin ratio of 10:1. Overnight incubation at 37 °C afforded a series of peptides which were prepared using PierceTM C18 spin columns according to the manufacturer's procedure.

The resulting peptide mixture was analysed by high resolution nESI FT-ICR MS using a 12 Telsa Solarix 2XR mass spectrometer (Bruker Daltonics) equipped with a nanomate infusion robot (Advion Biosciences). The resulting mass spectra were then processed using the SNAP algorithm in Data Analysis (Bruker Daltonics) to produce monoisotopic mass lists. The mass lists were then searched against the primary amino acid sequence of *Pf*CLK3 kinase domain$_{343\text{-}699}$ using MS-Fit in Protein Prospector (University of California, San Francisco) and ProSight Lite v1.4 (Northwestern University). For all analyses, error tolerances of 10 ppm were used. This analysis resulted in identification of 523 peptides, representing 59% sequence coverage.

The analysis indicated that three peptides (YSVVCELVGK, NITCDLLEHQYWLK, and YGNGHGLNATAVHCYTK) had been modified by a single neutral monoisotopic mass 482.195405, corresponding to the covalent adduct product of compound **4** ($C_{28}H_{26}N_4O_4$). Of these three peptides, the relative abundance of one (YSVVCELVGK) was orders of magnitude higher than the other two (6.2×10^8 vs 1.0×10^7 and 1.9×10^7). In order to confirm the modification of this peptide, the peptide was isolated and fragmented using collision induced dissociation (CID). Fragmentation confirmed the peptide sequence and located the modification to the residue Cys368.

Time resolved Förster resonance energy transfer (TR-FRET) assay. To a black 384-well plate was added 2.5 µL of each concentration of inhibitor serially diluted 1 in 3, 11 times from a

40 µM (4x) top concentration normalised to 4% DMSO, and 5 µL 50 nM (2x) recombinant *Pf*CLK3. Both were dissolved in kinase buffer (50 mM HEPES 7.4, 1 mM EGTA, 1 mM $MgCl_2$, 0.01% Tween and 1 mM TCEP). After a 15 minute preincubation, 2.5 µL of substrate mix (20 µM/ 2 mM / 12 mM ATP, 200 nM MBP in kinase buffer) was added [MBP sequence: CFFKNIVTPRTPPPSQGK]. Plates were sealed and centrifuged at 1000 rpm for 1 minute, and incubated at 37 °C for 2 hours. 5 µL of detection mix (30 mM EDTA, 3 nM AntiMBP in 1x Perkin Elmer Lance® detection buffer) was added to quench the kinase reaction, and plates were incubated at room temperature in the dark for 1 hour. Emission of the acceptor was then read using a PHERAstar fluorescence plate reader, and the results ($\frac{Emission\ 665\ nm}{Emission\ 620\ nm}$) were normalised to the no inhibitor (positive) and no protein (negative) controls via ($\frac{No\ inhibitor - Well}{No\ inhibitor - No\ protein}$) to give % inhibition. Each concentration was performed in triplicate, and each experiment was repeated 3 times. All 9 enzymatic reactions were then grouped, and a nonlinear regression curve with four parameters was then plotted using GraphPad Prism, generating activity data.

Thermal shift. To 384-well thermal shift plate was added 5 µL Protein Thermal Shift™ Buffer (Thermo Fisher Scientific), 5 µg full length *Pf*CLK3 (4.17 µL, 1.2 mg/mL), 8.13 µL Thermal Shift™ Buffer (Thermo Fisher Scientific), 0.2 µL 10 mM compound or vehicle (DMSO) and 2.5 µL Protein Thermal Shift™ Dye (Thermo Fisher Scientific) in triplicate. The plate was then sealed and heated from 5-95 °C over 15 minutes using QuantStudio^5 5 Qpcr (Thermo Fisher Scientific). Fluorescence was recorded as proteins unfolded. The Boltzmann distribution was calculated and T_m obtained using Protein Thermal Shift™ Software v1.4 (Thermo Fisher Scientific).

574 ***P. falciparum* culture and synchronisation.** *P. falciparum* cultures were maintained in RPMI-
575 1640 media (Invitrogen) supplemented with 0.2% sodium bicarbonate, 0.5% Albumax II, 2.0
576 mM L-glutamine (Sigma) and 10 mg/L gentamycin. For continuous culture, the parasites were
577 maintained at 4% haematocrit in human erythrocytes from 0+ blood donors and between 0.5 -
578 3% parasitaemia in an incubator at 37 °C, 5% carbon dioxide (CO_2), 5% oxygen (O_2) and 90%
579 nitrogen (N_2). To obtain highly synchronous ring stage parasites for assays, cultures were double
580 synchronised using Percoll and Sorbitol synchronisation. First, highly segmented schizonts were
581 enriched by centrifugation on a 70% Percoll (GE Healthcare) cushion gradient. The Schizont
582 pellet was collected and washed twice before fresh erythrocytes were added to a final
583 haematocrit of 4%, and incubated for about 1-2 hours shaking continuously to allow merozoites
584 egress and re-invasion of new erythrocytes. Residual schizonts were then removed by a second
585 Percoll purification followed by treating the ring pellet with sorbitol to generate highly
586 synchronous 1-2 hours old ring-stage parasites.

587 **Ex vivo *P. falciparum* inhibition assay.** To determine the IC_{50} of the molecules in parasites (*P.*
588 *falciparum* 3D7) ex vivo, the molecules were diluted 1 in 3 from a starting concentration of 100
589 µM for 12 dilution points. 50 µL of freshly diluted drugs, at twice the required final
590 concentrations were aliquoted into black 96-well plates. To the compound plates, 50 µL of
591 parasites prepared at 8% haematocrit at a parasitaemia (0.3 - 0.5%) were added and mixed by
592 pipetting up and down several times giving a final culture volume of 100 µL at the required
593 compound concentration (top concentration of 100 µM) and 4% haematocrit. To the 'no
594 compound' control, growth media was added and uninfected erythrocytes were included on the
595 plate as blank. The outer wells were filled with media to reduce evaporation from the
596 experimental wells and the plates incubated for 72 hours (±2 hours) to allow the parasites

sufficient time to re-invade before they are collected and frozen. For cellular washout studies, compound media was exchanged for compound-free media after 6 hours, and the parasites incubated for a further 66 hours. To quantify growth inhibition, the plates were thawed at room temperature for at least 1 hour and 100 µL of lysis buffer (20 mM Tris-HCl; 5 mM EDTA; 0.004% saponin and triton X-100) in PBS containing Sybr Green I (1µL in 5 ml) was added to each well and mixed by pipetting up and down several times and incubated for 1 hour in the dark shaking. Using a Fluroskan/ClarioStar plate reader at excitation of 485 nm and emission of 538 nm, plate absorbances were acquired. The data was normalised against the controls and graphs were generated using Graph Pad Prism 8 to determine the IC_{50} values using the non-linear regression log (inhibitor) versus response (three parameter) curve.

Selectivity assay. Compounds were evaluated using Eurofins Discovery's KinaseProfiler™ Diversity Panel of 58 representative kinases. KinaseProfiler™ is a radiometric assay using [γ-^{33}P]-ATP to measure phosphorylation of individual kinase substrates. A representative protocol for Abl is given below. Further details can be found by visiting the Eurofins Discovery Website.

Abl (h) is incubated with 8 mM MOPS pH 7.0, 0.2 mM EDTA, 50 µM EAIYAAPFAKKK, 10 mM Magnesium acetate and [γ-^{33}P]-ATP (specific activity and concentration as required). The reaction is initiated by the addition of the Mg/ATP mix. After incubation for 40 minutes at room temperature, the reaction is stopped by the addition of phosphoric acid to a concentration of 0.5%. 10 µL of the reaction is then spotted onto a P30 filtermat and washed four times for 4 minutes in 0.425% phosphoric acid and once in methanol prior to drying and scintillation counting.

CDK11 (CDK19) and CDK8 which have residues equivalent to C368 were then evaluated using the KINOME*scan*™ technology. Kinase-tagged T7 phage strains were prepared in an E. coli host derived from the BL21 strain. E. coli were grown to log-phase and infected with T7 phage and incubated with shaking at 32 °C until lysis. The lysates were centrifuged and filtered to remove cell debris. The remaining kinases were produced in HEK-293 cells and subsequently tagged with DNA for qPCR detection. Streptavidin-coated magnetic beads were treated with biotinylated small molecule ligands for 30 minutes at room temperature to generate affinity resins for kinase assays. The liganded beads were blocked with excess biotin and washed with blocking buffer (SeaBlock (Pierce), 1% BSA, 0.05% Tween 20, 1 mM DTT) to remove unbound ligand and to reduce non-specific binding. Binding reactions were assembled by combining kinases, liganded affinity beads, and test compounds in 1x binding buffer (20% SeaBlock, 0.17x PBS, 0.05% Tween 20, 6 mM DTT). Test compounds were prepared as 111X stocks in 100% DMSO. K_d was determined using an 11-point 3-fold compound dilution series with three DMSO control points. All compounds for K_d measurements are distributed by acoustic transfer (non-contact dispensing) in 100% DMSO. The compounds were then diluted directly into the assays such that the final concentration of DMSO was 0.9%. All reactions performed in polypropylene 384-well plate. Each was a final volume of 0.02 mL. The assay plates were incubated at room temperature with shaking for 1 hour and the affinity beads were washed with wash buffer (1x PBS, 0.05% Tween 20). The beads were then re-suspended in elution buffer (1x PBS, 0.05% Tween 20, 0.5 μM nonbiotinylated affinity ligand) and incubated at room temperature with shaking for 30 minutes. The kinase concentration in the eluates was measured by qPCR.

Cytotoxicity assay. HepG2 cells were cultured in Dulbecco's Modified Eagle Medium (DMEM) with 10% fetal bovine serum and maintained in the exponential stage at 1-200,000 cells/mL.

Cells were detached using 0.05% trypsin-EDTA. Cultures were incubated at 37 ℃, 5% CO_2. 96 well plates were seeded at 10,000 cells/well and incubated for 24 hours. Media was then exchanged for compound media (serial dilutions from 300 μM to 37 nM, or 100 μM to 25 nM) and incubated for 48 hours. Compound media was then exchanged for unmodified media, 10% alamar blue. Plates were then incubated for 4 hours and analysed using a Clariostar™ plate reader and the Flourescence Intensity (540-20 nM/590-30 nM) was measured. Each concentration was plated in triplicate, and 3 controls containing DMSO only, no alamar blue and no cells were also plated in triplicate. Values were normalised to give percentage inhibition using the no cells control as 100% inhibition and the DMSO control as 0% inhibition. Experiments were performed 3 times and all 9 wells were then grouped, and a nonlinear regression curve with four parameters was then plotted using GraphPad Prism, generating activity data.

Data availability

The following data is available online in supplementary information: Data for X-ray structure determination; experimental procedures and characterization data for all compounds; copies of ^{1}H, ^{13}C, NMR spectra for all compounds; analytical HPLC traces for final compounds; thermal shift assays; metabolic stability assays; selectivity data and analysis of key compounds.

Code availability

No code was generated for this study

Acknowledgements

The authors acknowledge the use of the Advanced Photon Source for structural data collection and thank the staff for their support. The authors also thank Amanda Mackenzie of KelticPharma

for her consultation and advice throughout the project. D.J.C. thanks the U.K. Biotechnology and Biological Sciences Research Council (BBSRC) for supporting high resolution mass spectrometry instrumentation used in this study [BB/R013993/1]. S.B.B. thanks the EPSRC for studentship (EP/T517896/1 and EP/W524359/1).

Author Contributions

S.B.B., A.G.J., A.B.T and G.M. conceived the study and analysed data. S.B.B. and A.G.J. designed the inhibitors. S.B.B. performed molecular modelling, synthesised and characterised compounds, and performed GST assays. R.G. carried out reaction optimisation. S.B.B. and D.J.C. performed and analysed protein and peptide mass spectrometry. S.B.B., A.B. and G.C. carried out protein kinase activity experiments. S.B.B., M.J.C and A.B. carried out human tissue culture and cell viability experiments. O.J., S.S., and N.O. carried out culture and testing of compounds in *Pf* parasites. B.A., S.B.B. and M.J.C. carried out protein purification and optimisation. T.Y. and A.J.H. performed protein crystallisation and X-ray data collection. S.B.B. wrote the manuscript, and all authors contributed to manuscript editing.

Competing interests

A.G.J. and S.B.B. are inventors on a provisional patent (008521262) filed by the University of Glasgow on covalent anti-malarial inhibitors and their analogs that target *Pf*CLK3. A.B.T., A.G.J. & G.M. are share holders of and receive consultancy payments from Keltic Pharma Therapeutics Ltd. The other authors declare no competing interests.